Transient Electric Birefringence Measurements of the Rotational and Internal Bending Modes in Monodisperse DNA Fragments

Roger J. Lewis and R. Pecora*

Department of Chemistry, Stanford University, Stanford, California 94305

Don Eden

Department of Chemistry, San Francisco State University, San Francisco, California 94132.
Received June 26, 1985

ABSTRACT: We report electric birefringence measurements on four blunt-ended DNAs 367, 762, 1010, and 2311 base pairs in length. The multiexponential zero-field birefringence decay was resolved into separate components by automatic computer programs that do not require any a priori knowledge of the number of decay processes existing in the data. The slowest of these components represents the rotational motion of the molecule and is in good agreement with the experimental work of Stellwagen (*Biopolymers* **1981**, *20*, 399) and the theoretical and experimental work of Hagerman and Zimm (*Biopolymers* **1981**, *20*, 1481, 1503). The next faster mode occurs 3–7 times faster than the rotational mode, approximately at the rotational time that would be expected for the rotation of a semistiff polymer half the overall length of the molecule. The spacing between the rotational and internal modes is reduced in the longer DNAs. The faster mode probably represents the longest wavelength internal bending of the DNA. The frequency spacing of the rotational and first internal modes is favorably compared with that predicted by the "trumbell" model of Roitman and Zimm (*J. Chem. Phys.* **1984**, *81*, 6348) and the Rouse–Zimm model as developed by Zimm (*J. Chem. Phys.* **1956**, *24*, 269) and Zimm et al. (*J. Chem. Phys.* **1956**, *24*, 279). The spacing between the first and second internal bending modes is compared with the predictions of the recent model of Aragôn and Pecora (*Macromolecules* **1985**, *18*, 1868).

Introduction

Transient electric birefringence is a powerful technique for studying the motions of optically anisotropic molecules in solution.[1-3] In recent years, many investigators have studied the rotational motion of DNA by electric birefringence, both experimentally[4-11] and theoretically.[12-17] Despite this work, the electric field orientation mechanism in DNA is still poorly understood.[4,9,10,12-20] In addition, work on electric dichroism[7,21] and magnetic birefringence[22] of DNA has also appeared. In the present work we concern ourselves primarily with the zero-field relaxation of the electric birefringence of the DNA.

Advances in recombinant DNA technology have made it possible to obtain monodisperse samples of DNA for which the entire nucleotide sequence is known.[23,24] The detailed characterization and reproducibility of these systems make them ideal for study. Small DNA molecules, below approximately 100 base pairs (bp) in length, show rotational behavior similar to that of a rigid rod.[4-8] Longer DNA fragments show faster rotational motion than that expected for a rigid rod because of flexibility and, in addition, may show multiexponential birefringence decays, presumably because of internal motions. In the work that follows, we will often refer to the slowest time observed in the birefringence decay as the "rotational" time despite the fact that, for semiflexible molecules, the slowest decay mode probably involves coupled rotational and bending motions. Several workers, notably Elias and Eden,[4,5] Hagerman,[6] Diekmann et al.,[7] and Stellwagen,[8] have separated the long-time behavior of these molecules from the internal modes in order to accurately measure the rotational time of the molecules. These measurements of the rotational time have been compared to various theoretical predictions for rigid[25-32] and flexible rods[33,34] in order to obtain a measurement of the persistence length of the DNA.

The theoretical work of Hagerman and Zimm[33] on the rotational diffusion constant of semiflexible polymers overcame many of the limitations of the pioneering work by Hearst.[34] Because of this work, the effects of flexibility on the rotational diffusion constant of DNA fragments are now reasonably well understood for molecules with dimensions up to four or five persistence lengths (about 600–800 bp).

The faster relaxations observed in the birefringence and dichroism decays are more difficult to characterize experimentally than those due to rotational motion, and, of the above workers, only Diekmann et al.[7] attempted any quantification of their decay times. Using pulses of strength 10–70 kV/cm, they found that for small DNA fragments (below about 260 bp in length) their data could be adequately represented by two exponentials, one representing rotational motion and the other the slowest internal bending of the DNA. The magnitude of the faster relaxation increased with the strength of the orienting field. For larger DNAs (greater than about 600 bp in length) they found that they needed three or even four exponentials to represent the data. Because of the complexity of the birefringence decay, they were unable to characterize either the rotation or the internal motions of these larger molecules.

We have measured the zero-field decay of the transient electric birefringence for blunt-ended restriction fragments 367, 762, 1010, and 2311 bp in length using a variety of pulse widths at reasonably low field strength in dilute solution. A multiexponential analysis program, DISCRETE,[35,36] and a constrained inverse Laplace transform program, CONTIN,[37-39] have been used to determine the number of exponentials needed to represent the data and their decay times. These results are compared to various theoretical models, whose basic properties are reviewed in the next section.

Models of Rotational Motion

In 1962, Hearst[34] calculated the rotational diffusion constant for a wormlike coil and weakly bending rod using a bead model. He accounted for the hydrodnamic interactions between the beads by preaveraging the Oseen hydrodynamic interaction tensor over a cylindrically symmetric distribution of chain configurations. His result for the rotational diffusion constant is defined in terms of the radius of each frictional element, the distance between frictional elements, and the persistence length of the molecule. Although the model fits data from DNA to yield

0024-9297/86/2219-0134$01.50/0

Table I
Ratios of λ_2 to λ_1 for "Trumbell" Model of Roitman and Zimm[38]

stiffness parameter (Z)	first internal eigenvalue (λ_2)	rotational eigenvalue, (λ_1)	(λ_2/λ_1)
1.25	27.55	3.544	7.8
1.00	23.83	3.674	6.5
0.75	20.41	3.870	5.3
0.50	17.26	4.177	4.1
0.25	14.54	4.667	3.1

reasonable values for the persistence length,[4] the precise physical interpretation of the first two parameters is ambiguous.

Hagerman and Zimm[33] approached the same problem by creating an ensemble of shapes using the Monte Carlo method and by evaluating the friction and the Oseen interaction tensors for rotations about the center of mass, whose position is easily determined. This approach avoids the preaveraging approximation. By making a small correction for the different positions of the center of mass and the center of hydrodynamic resistance, Hagerman and Zimm were able to calculate the rotational diffusion constant for wormlike chains up to five persistence lengths. Their result is expressed as a function of the rotational diffusion constant predicted by a Broersma relation[27,28] for a rigid rod of the same dimensions and the ratio of the overall length to the persistence length.

Models of Internal Motion

Roitman and Zimm[40-42] have calculated the expected dynamics for a "trumbell", which consists of three beads connected together by two rigid bonds. The structure bends at the center bead, subject to a restoring force, whose strength is measured by a parameter Z. Building upon some earlier work by Hassager,[43,44] Roitman and Zimm determined the eigenfrequencies of the normal modes. This analysis included the effects of the hydrodynamic interaction between the beads. Their analysis for electric birefringence[41] assumes that the orientation mechanism is simply the anisotropic polarizability of each of the bonds. This is surely an oversimplification for the case of DNA,[4,7-10] a polyelectrolyte. The slowest mode expected in the electric birefringence decay from the trumbell consists of a nearly rigid end over end rotation. As expected, this mode slows down and eventually becomes rigid rotation as the restoring force constant, Z, is increased.

The next normal mode consists of a coupled rotational–bending motion. The frequency of this mode increases as Z is increased. As the first mode decreases in frequency with Z and the second increases, the spacing of these modes is a sensitive function of the strength of the restoring force at the center bond.[42] "Spacing" here and subsequently refers to the ratio of the decay times for two processes. Table I shows the expected spacing as a function of the parameter Z.

Recently, Aragón and Pecora[45] developed a model for the internal dynamics of a semistiff polymer by separating the translational and rotational motions from the internal dynamics and then solving for the normal modes of the semiflexible rod. No correction is made for the hydrodynamic interactions between different sections of the molecule. This model makes predictions for the length dependence and the ratio of the decay times for the first and second internal bending modes of the polymer that are independent of the value of the persistence length, as long as the persistence length is independent of molecular weight. Specifically, it predicts that the spacing of the first and second internal modes should be equal to the fourth power of their respective bending eigenvalues, giving a spacing of 7.60. It also predicts that the decay time for a particular internal mode will increase as the fourth power of the contour length.

The Rouse–Zimm model[46,47] for the dynamics of an infinitely flexible chain is well-known. The first two modes of the chain have decay times that we shall call τ_1 and τ_2, respectively. Hearst[34] has suggested that his rotational time for a semiflexible polymer should be compared with Zimm's τ_1. In that case, the spacing between the rotational and first internal modes of a semistiff polymer would be analogous to the spacing between τ_1 and τ_2. In the free-draining limit the ratio of these times is 4 exactly,[46] while in the non-free-draining limit the ratio is 3.17.[47] Rau and Bloomfield[9] and Harrington[48] have both obtained evidence that very large DNAs may well appear to be essentially free draining.

Each of these models, whose predictions we will compare with our experimental results, is suitable for modeling the internal dynamics of DNA in different molecular weight regions. The trumbell model, with a relatively large parameter Z, would be best suited for modeling the rotation and first internal bending mode of short DNA, which is quite stiff. Longer DNAs would require a correspondingly smaller parameter Z.[41] The Aragón–Pecora theory is suitable as a model for the first and second internal modes of small DNAs. For longer DNAs, the assumption of uncoupled rotational and internal modes used in that model is probably less valid, as the two motions will occur on the same time scale. The Rouse–Zimm model is most applicable for very long DNAs because of their extreme contour length.

Experimental Methods

DNA fragments of length 367, 762, 1010, and 2311 bp were prepared as previously described.[24] The 367-bp sample actually consists of equimolar amounts of DNA fragments 27, 367, and 368 bp in length.[24] Because the 27-bp fragment corresponds to approximately 3.5% of the DNA by weight and its decay times would be much faster than those we wished to measure,[25-30] no attempt was made to remove it from the sample. The DNA fragments were ethanol precipitated and resuspended in sodium phosphate buffer (1 mM in phosphate) at pH 7.0 at a concentration of approximately 15–20 μg/mL. The solutions were then dialyzed for 8 h against four changes of the same buffer at 0 °C. The absorbance at 260 and 280 nm was measured, and the DNA was diluted with the same buffer to a concentration of 5 μg/mL for the two smaller fragments and 10 μg/mL for the two larger fragments. Prior to the electric birefringence measurements the impedance of the samples was measured at 1 kHz. These measurements indicated that the actual ionic strength of the samples varied from about 1.5 to 3 mM in sodium. Although this is a larger variation than we expected, it is reassuring to note that recent work[6] suggests that the persistence length of DNA is relatively constant in this ionic strength region.

The electric birefreingence apparatus has been described previously.[18,49] Data, taken at 20 °C, were averaged over 5000 pulses. The duration and strength of the pulses are listed in Table II. This technique of varying the orienting pulse width, with the aim of differentially exciting different dynamic modes, has been reported previously.[49]

The collected data were converted to birefringence units and transferred to a Universe 68 computer, a M68000-based system manufactured by Charles River Data Systems. The zero-field decay section of the data was normalized and multiplied by −1 so that nonnegativity constraints on the amplitude of the exponential decays could be applied during the data analysis. The data were then analyzed by DISCRETE and CONTIN.

DISCRETE,[35,36] a Fortran program written by Provencher, analyzes data in terms of a discrete sum of exponential decays. It statistically determines the minimum number of exponential decays that are required to fit the data given the noise in the data. In our case we assumed the amplitudes of the exponentials were

Table II
Strength and Duration of Orienting Pulses

DNA length, bp	pulse duration, μs	field strength, V/cm
367 (mol wt = 2.4 × 10^5)	50	1100
	2	1850
762 (mol wt = 5.0 × 10^5)	300	740
	20	1100
	2	1850
1010 (mol wt = 6.7 × 10^5)	400	460
	50	560
	5	1480
2311 (mol wt = 1.52 × 10^6)	1000	460
	100	740
	10	1850

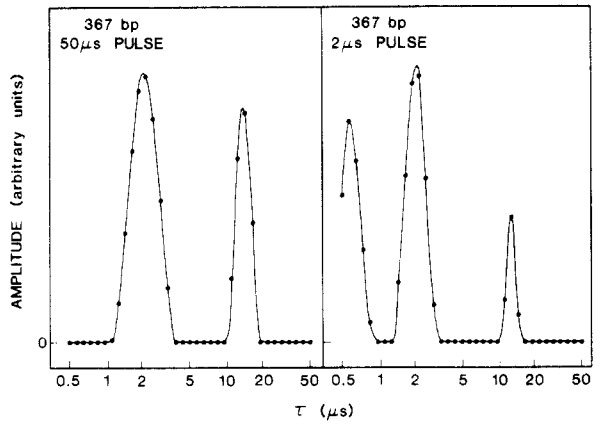

Figure 1. This figure shows the fully smoothed CONTIN analyses of the zero-field birefringence decay of the 367-bp fragment. With a 50-μs orientation pulse, CONTIN is able to resolve two separate components in the decay. The slow component at 14.4 μs comprises 75% of the amplitude and the faster component at 2.3 μs comprises the rest of the decay amplitude. Amplitudes, corresponding to the areas under the peaks, are difficult to judge visually because of the logarithmic scale on the abscissa. With a 2-μs pulse, CONTIN resolves the same modes as before with the addition of an even faster mode around 0.5 μs.

positive and that there was an additive constant whose sign was unconstrained. If the data actually contained a continuous distribution of decay times, for example data from a polydisperse system, DISCRETE would still find the minimum number of discrete exponentials required to fit the data, but this number may be larger than the number of distinct decay processes that are actually occurring. Thus, DISCRETE cannot be used to determine the number of distinct decay processes in very polydisperse systems.

CONTIN,[37-39] also written by Provencher, analyzes data in terms of a continuous distribution of exponential decay times. It determines the smoothest distribution of decay times that adequately fits the data. When data are of insufficient precision to prove the existence of distinct decay modes, CONTIN's solution will show a wide monomodal distribution of decay times.[50] This process of searching for the smoothest distribution of decay times ensures that CONTIN will not exaggerate the number of distinct decay processes occurring in data containing a wide distribution of decay times.

Obviously, if one has the additional a priori information that the system under examination is monodisperse, implying that the data consist of a discrete sum of exponentials, then analysis with DISCRETE should yield more information about the system.

Results

The CONTIN analysis of the birefringence decay data from the 367-bp fragment is presented in Figure 1. After a 50-μs orienting pulse, during which the birefringence reaches steady state, there are essentially two decay processes. The slower of the two, at 14.4 μs, corresponds to 75% of the amplitude, while the faster, at 2.3 μs, represents

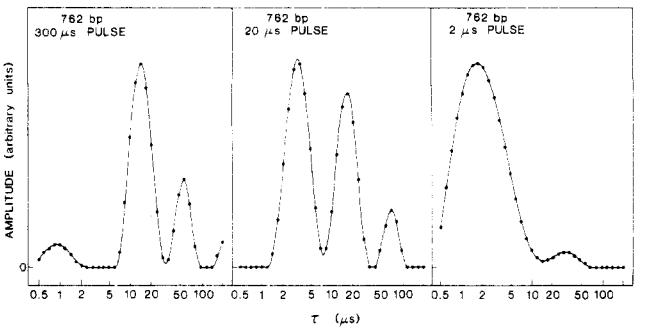

Figure 2. This figure shows the CONTIN analyses of the data from the 762-bp fragment. See text for discussion.

the other 25%. The slower decay process is rotation while the faster is an internal bending mode. When the same DNA is oriented with a 2-μs pulse and the data are collected at a faster sampling interval (every 80 ns vs. 160 ns), CONTIN is able to resolve three relaxation processes. The rotational peak is still apparent at 13–14 μs, but it now contributes approximately 50% of the decay amplitude. The first internal mode appears at a position slightly slower than 2 μs, representing another 45% of the amplitude. In addition, a third peak appears at approximately 0.5 μs, making up the rest of the decay amplitude. The amplitude and position of the fastest decay process varied from data set to data set, between 5% and 25% of the amplitude with decay times of 0.4–1.3 μs. This variability is consistent with our previous experience[51] with CONTIN and the analysis of multiexponential decay processes. Evidently the data are not sufficiently accurate to resolve the fastest of three exponentials with better precision.

A number of generalizations may be drawn from the data on the 367-bp fragment. First of all, the locations of the rotational and first internal decays were not affected by the length of the orienting pulse. This is in sharp contrast to observations made by Stellwagen.[8] Second, the shorter orientation pulse selectively excited the faster modes, increasing the amplitude of the faster decays relative to slower decays when compared with the steady-state case.

Figure 2 shows the CONTIN analysis of birefringence data frm the 762-bp fragment. With a 300-μs orienting pulse we detected two significant decay processes. The rotational peak occurred around 75 μs and constituted 51% of the decay amplitude; the next faster process at 18 μs made up another 45% of the amplitude. The small peak around 0.5–2 μs is probably an artifact[51] as the data collection sample time was 1 μs. The small peak at the largest decay time appeared intermittently during the fitting of data from this DNA but did not affect the location of the two principal peaks. With a 20-μs pulse we excited three modes, the first two being identical with those found with the 300-μs pulse. The fastest mode occurred around 2–5 μs, but its location was variable. It probably represents the second internal bending mode in the DNA. With a 2-μs pulse it was not possible to obtain data of sufficient precision to reproducibly resolve the decay modes. The last panel in Figure 2 shows a typical result. The small peak at 20–50 μs probably represents the very slightly excited rotational and first internal modes. The faster internal modes are represented by the large peak extending from 0.5 to 5 μs, but it is impossible to determine any fine structure from the analysis. As in the case of the 367-bp fragment, the shortest pulse lengths excited the slowest mode to a lesser extent.

The CONTIN analysis of the birefringence data from the 1010-bp fragment is shown in Figure 3. With the longest

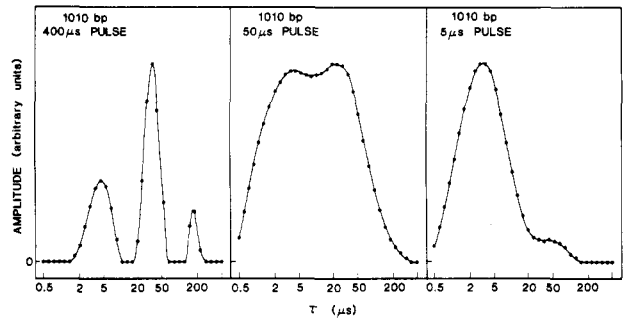

Figure 3. This figure shows the results from the 1010-bp fragment. See text for discussion.

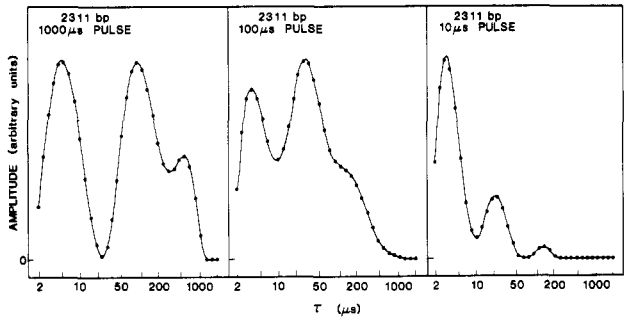

Figure 4. This figure shows the results from the 2311-bp fragment. In this case CONTIN was unable to demonstrate the existence of separate decay modes. These undersmoothed solutions represent best fits to the data, but they may contain more information than is justified by the precision of the data. The results are consistent with the analyses by DISCRETE, as expected. See text for discussion.

orientation pulse again we see a slow rotational decay (179 μs, 41% of the decay) and a faster internal bending mode (40 μs, 54% of the decay). The fastest mode, around 5 μs, may or may not be significant as the data collection sample time was 1.5 μs. It represents the other 5% of the decay. With a shorter orientation pulse, 50 μs, we seem to excite many modes relatively evenly and CONTIN is unable to resolve the decays from each other. With a 5-μs orientation pulse only the internal modes are excited, with the amplitude of the second internal mode much larger than that of the first internal mode.

Figure 4 shows the CONTIN analysis of the birefringence data from the 2311-bp fragment. The dynamic spectrum from this DNA appears to be so complex that CONTIN is unable to unambiguously resolve the components. The analyses shown are deliberately "undersmoothed",[39] meaning that although they are the best fit to the data, they may well contain more detail than is justified by the precision of the data. With a 1000-μs pulse, the rotational peak is around 670 μs and the first internal bending mode is around 170 μs. The peak at 5–10 μs is insignificant as the data collection sample time was 4 μs. With a 100-μs pulse, rotation seems to remain unexcited and the first internal decay mode appears as a "shoulder" on the peak at approximately 40 μs. The peak at 40 μs is probably the second internal bending mode. With a very short orientation pulse, 10 μs, we see three decay modes, which probably represent the first, second, and third internal bending modes. It is important to remember that these are undersmoothed solutions and that the detail shown in them may not be justified by the precision of the data.

DISCRETE, which assumes the decay consists of a discrete sum of exponentials, is capable of a more consistent analysis of the data from the larger fragments. We believe the assumption of discrete decay processes is justified by the CONTIN analysis of the smaller three fragments, which show fully resolved decay processes. The average positions of the decay processes using all pulse widths, as analyzed by DISCRETE, are shown in Table III.

Table III
Rotational and Internal Mode Decay Times As Analyzed by DISCRETE[32,33]

DNA length, bp	rotational decay time, μs	first internal decay time, μs	second internal decay time, μs
367	14.4	2.3	<1.0
762	78	16.5	2–4
1010	171	37	5–6
2311	688	204	40–60

Table IV
Predicted[33] and Observed Rotational Times

DNA length, bp	rotational time, μs			
		predicted		
	obsd	P = 500 Å	P = 700 Å	P = 1000 Å
367	14.4	13.9	16.5	
762	78	59.2	77.0	97.0
1010	171		134.0	175

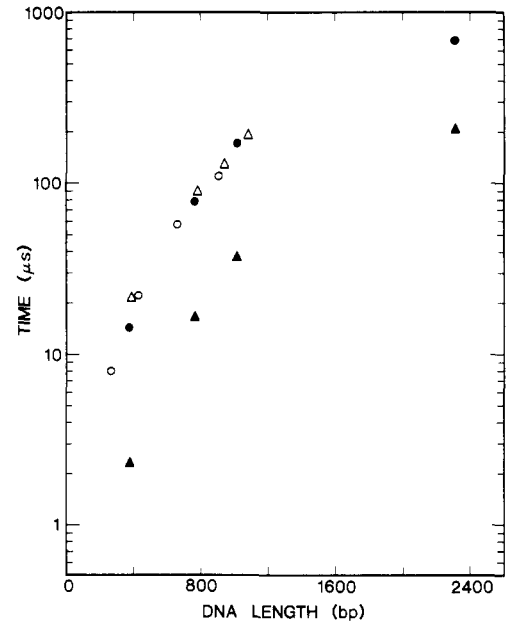

Figure 5. This figure shows the decay times for the rotation of DNA restriction fragments and the first internal bending mode. The open circles are from the work of Hagerman[6] and the open triangles are from the work of Stellwagen.[8] Our results for the rotational time are shown by the solid circles, and our results for the first internal mode are shown by the solid triangles. All measurements were either taken at or corrected to 20 °C.

It is important to determine that these data analysis programs are accurately separating the decay modes from each other. In order to demonstrate this, we may compare our slowest relaxation times, the rotational decays, with the rotational decays observed by other workers on DNAs of similar length. Figure 5 shows our results for the rotational and first internal modes in comparison with Hagerman's[6] and Stellwagen's[8] results. Despite the different ionic strengths and procedures used by each worker, the results for the rotational decay agree within the experimental uncertainties. This suggests that CONTIN and DISCRETE are, in fact, accurately resolving the decay modes from each other.

If we compare our results for the rotational decay times with the prediction of the model of Hagerman and Zimm,[33] we find that we cannot account for the data from each of

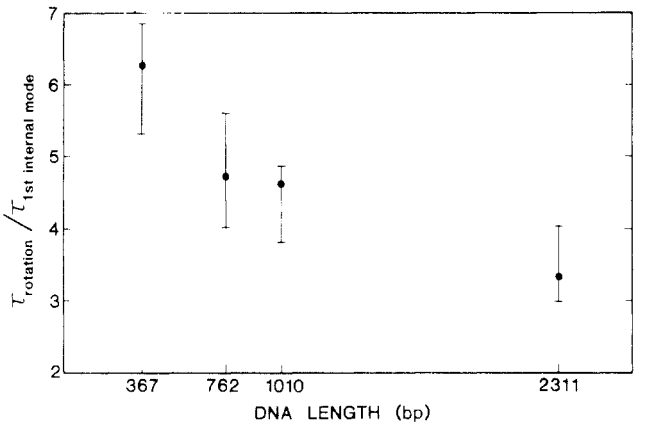

Figure 6. This figure shows the ratio of the rotational decay time to that of the first internal mode as a function of DNA length. The error bars show the limits of the worst-case errors; i.e., the upper end of the bar shows the ratio of the longest measured rotational time in any run to the shortest observed first internal mode. Despite this conservative error estimate, it is clear that there is a significant trend toward a closer spacing of the modes as the DNAs increase in length. This is consistent with the model of Roitman and Zimm[40] (see text).

the three smallest fragments using a single value for the persistence length (see Table IV). Here we have assumed that the hydrodynamic diameter of the DNA is 26 Å and the rise per base pair is 3.36 Å.[52]

These data suggest that either the persistence length is a function of the length of the DNA or the model of Hagerman and Zimm is less applicable for the longer DNAs. It is quite possible that the theoretical assumption of rigid rotation used in the model is less valid for the longer DNAs. The suggestion that electrostatic end effects may reduce the apparent persistence length in short DNA fragments has been made by Hagerman.[53]

As was mentioned previously, the spacing of the rotational and first internal modes in the trumbell model is a function of the stiffness of the center bond. Figure 6 shows the ratio of the rotational to first internal decay times as a function of the length of the DNA. It is clear from the data that the two modes become more closely spaced in the longer DNAs. As discussed in the article by Roitman and Zimm,[40] longer DNAs would be expected to exhibit behavior corresponding to a lower stiffness parameter Z. The mode spacing in the 367-bp fragment suggests a stiffness parameter around 1.0, while the spacing in the 2311-bp fragment corresponds to a stiffness parameter around 0.3 (see Table I). Thus the experimental data confirm two predictions of the trumbell model. First of all, the spacing is approximately correct, ranging from approximately 6.3 to 3.4. Second, the spacing is reduced as the DNAs increase in length.

Although the trumbell model is obviously an oversimplification of the dynamical behavior of DNA, it is not surprising that the model fits the rotational and first internal mode spacing reasonably well. We suspect that the slowest internal normal mode in the DNA probably corresponds to a bending motion that is not too dissimilar from the first internal motion of the model itself. Comparing faster internal modes of the DNA with the trumbell model would probably not be as fruitful, as these internal modes would correspond to motions forbidden by the rigid sections of the model.

The model of Aragón and Pecora[45] can be compared with the higher order modes, however. Unfortunately the accuracy of the data does not allow very accurate determination of the decay time for the second internal bending mode. The approximate values are listed in Table III. We see that the ratio of the decay times for the first and second internal bending modes is somewhere between 6 and 8 for the 762- and 1010-bp fragments. The ratio predicted by the theory, as mentioned above, is 7.60. Within the error of the measurements, the data agree with the theoretical prediction for these two fragments. With the longer 2311-bp fragment, however, the ratio is between approximately 3.4 and 5.1, in disagreement with the theoretical prediction. It is perhaps not surprising that the theory is less successful in predicting the dynamics of the largest fragment as the theoretical assumption of uncoupled rotational and internal modes is probably less valid as the DNAs increase in length.

A second prediction of the Aragón and Pecora model[45] is that the decay times of the internal modes will increase proportionally to the contour length to the fourth power. Although the data on the first internal mode for the 762- and 1010-bp fragments are marginally consistent with this prediction, comparison of the data on the first internal mode for the 367- and 762-Bp fragment is certainly inconsistent with it. Obviously more accurate data will be required to determine the length dependence and spacing of the first and second internal bending modes in DNA.

In the case of the longest DNA, it is interesting to compare the observed spacing of the rotational and first internal bending modes with the spacing of the first two internal times predicted by the Rouse–Zimm model for a flexible chain. The measured value for this spacing is 3.4 but the worst case uncertainty extends from 3.0 to 4.0. As mentioned above, a ratio of exactly 4 is theoretically predicted for the ratio of the first two times in the free-draining limit. A ratio of 3.17 is predicted for the non-free-draining limit. We believe that our data are only barely consistent with a ratio of 4, suggesting a probable hydrodynamic contribution to the spacing. Our data are completely consistent with the ratio predicted for the non-free-draining limit. These data suggest that, if the Rouse–Zimm model is applicable, this DNA appears to be closer to the non-free-draining limit than the free-draining limit.

Conclusions

In this work we have resolved the rotational and first internal birefringence decay times in monodisperse DNA samples. The results are consistent with the trumbell model of Roitman and Zimm[40-42] and approach the prediction of the Rouse–Zimm model[46,47] for the larger DNA.

The analyses by DISCRETE demonstrate that the birefringence decays of the larger fragments are consistent with separate decay processes with the relaxation times shown in Table III. Diekmann et al.[7] raise the question of whether or not the birefringence and dichroism decays of large DNA fragments consist of separate decay processes or a continuum of decay times. We have been able to obtain data that demonstrate the existence of separate decay processes on DNA as large as 1010 bp and are consistent with separate decay processes on DNA as large as 2311 bp. We believe that larger DNAs (for example, in the work of Diekmann et al., 4363 bp) would display dynamical behavior that is simply an extension of that observed here. In other words, we would expect a larger number of decay modes spaced relatively close together. This type of decay is notoriously difficult to analyze and it is not surprising that, despite an excellent approach, Diekmann et al. were unable to resolve the matter.

Acknowledgment. This work was supported by NIH Grant 2 RO1 GM 22517 and NSF Grants CHE82-00512 and CHE85-11178 to R.P. This work was also supported

by the NSF MRL Program through the Center for Materials Research at Stanford University. R.J.L. was supported by the NIH Medical Scientist Training Program at the Stanford University School of Medicine. D.E. was supported by NIH Grant 2 RO1 GM 31674 and a NIH Research Career Development Award 5 KO4 AM 01353. We acknowledge the valuable assistance of Susan Sorlie and Matheen Haleem.

References and Notes

(1) Fredericq, E.; Houssier, C. "Electric Dichroism and Electric Birefringence"; Clarendon Press: Oxford, 1973.
(2) Krause, S., Ed. "Molecular Electro-optics"; Plenum Press: New York, 1980.
(3) O'Konski, C. T., Ed. "Molecular Electro-optics"; Marcel Dekker: New York, 1976.
(4) Elias, J. G.; Eden, D. *Macromolecules* **1981**, *14*, 410.
(5) Elias, J. G.; Eden, D. *Biopolymers* **1981**, *20*, 2369.
(6) Hagerman, P. J. *Biopolymers* **1981**, *20*, 1503.
(7) Diekmann, S.; Hillen, W.; Morgeneyer, B.; Wells, R. D.; Porschke, D. *Biophys. Chem.* **1982**, *15*, 263.
(8) Stellwagen, N. C. *Biopolymers* **1981**, *20*, 399.
(9) Rau, D. C.; Bloomfield, V. A. *Biopolymers* **1979**, *18*, 2783.
(10) Stellwagen, N. C. *Biophys. Chem.* **1982**, *15*, 311.
(11) Marion, C.; Perrot, B.; Roux, B.; Bernengo, J. C. *Makromol. Chem.* **1984**, *185*, 1665.
(12) Marion, C.; Roux, B.; Bernengo, J. C. *Makromol. Chem.* **1984**, *185*, 1647.
(13) Yoshioka, K. *J. Chem. Phys.* **1983**, *79* (7), 3482.
(14) Diekmann, S.; Jung, M.; Teubner, M. *J. Chem. Phys.* **1984**, *80* (3), 1259.
(15) Wegener, W. A.; Dowben, R. M.; Koester, V. J. *J. Chem. Phys.* **1979**, *70* (2), 622.
(16) Rau, D. C.; Charney, E. *Macromolecules* **1983**, *16* (10), 982.
(17) Rau, D. C.; Charney, E. *Biophys. Chem.* **1983**, *7*, 35.
(18) Eden, D.; Elias, J. G. In "Measurement of Suspended Particles by Quasi-Elastic Light Scattering"; Dahneke, B. E., Ed.; Wiley: New York, 1983; p 401.
(19) Fixman, M. *Macromolecules* **1980**, *13*, 711.
(20) Fixman, M.; Jagannathan, S. *J. Chem. Phys.* **1981**, *75* (8), 4048.
(21) Hogan, M.; Dattagupta, N.; Crothers, D. M. *Proc. Natl. Acad. Sci. U.S.A.* **1978**, *75* (1), 195.
(22) Maret, G.; Weill, G. *Biopolymers* **1983**, *22*, 2727.
(23) Maniatis, T.; Fritsche, E. F.; Sambrook, J. "Molecular Cloning"; Cold Spring Harbor Laboratory: Cold Spring Harbor, New york, 1982.
(24) Lewis, R. J.; Huang, J. H.; Pecora, R. *Macromolecules* **1985**, *18*, 1530.
(25) Tirado, M. M.; Martinez, C. L.; Garcia de la Torre, J. *J. Chem. Phys.* **1984**, *81* (4), 2047.
(26) Broersma, S. *J. Chem. Phys.* **1981**, *74*, 6989.
(27) Broersma, S. *J. Chem. Phys.* **1960**, *32*, 1626.
(28) Broersma, S. *J. Chem. Phys.* **1960**, *32*, 1632.
(29) Tirado, M. M.; Garcia de la Torre, J. *J. Chem. Phys.* **1979**, *71*, 2581.
(30) Stimpson, D. I.; Bloomfield, V. A. *Biopolymers* **1985**, *24*, 387.
(31) Tirado, M. M.; Garcia de la Torre, J. *J. Chem. Phys.* **1980**, *73*, 1986.
(32) Newman, J.; Swinney, H. L.; Day, L. A. *J. Mol. Biol.* **1977**, *116*, 593.
(33) Hagerman, P. J.; Zimm, B. H. *Biopolymers* **1981**, *20*, 1481.
(34) Hearst, J. E. *J. Chem. Phys.* **1963**, *38* (5), 1062.
(35) Provencher, S. W. *Biophys. J.* **1976**, *16*, 27.
(36) Provencher, S. W. *J. Chem. Phys.* **1976**, *64*, 2772.
(37) Provencher, S. W.; Hendrix, J.; De Maeyer, L.; Paulussen, N. *J. Chem. Phys.* **1978**, *69* (9), 4273.
(38) Provencher, S. W. *Makromol. Chem.* **1979**, *180*, 201.
(39) Provencher, S. W. "CONTIN User's Manual"; European Molecular Biology Laboratory Technical Report EMBL-DAO2, Heidelberg, 1980.
(40) Roitman, D. B.; Zimm, B. H. *J. Chem. Phys.* **1984**, *81* (12), 6348.
(41) Roitman, D. B. *J. Chem. Phys.* **1984**, *81* (12), 6356.
(42) Roitman, D. B.; Zimm, B. H. *J. Chem. Phys.* **1984**, *81* (12), 6333.
(43) Hassager, O. *J. Chem. Phys.* **1974**, *60* (5), 2111.
(44) Hassager, O. *J. Chem. Phys.* **1974**, *60* (10), 4001.
(45) Aragón, S. R.; Pecora, R. *Macromolecules* **1985**, *18*, 1868.
(46) Zimm, B. H. *J. Chem. Phys.* **1956**, *24* (2), 269.
(47) Zimm, B. H.; Roe, G. M.; Epstein, L. F. *J. Chem. Phys.* **1956**, *24* (2), 279.
(48) Harrington, R. E. *Biopolymers* **1978**, *17*, 919.
(49) Highsmith, S.; Eden, D. *Biochemistry*, in press.
(50) Lewis, R. J., unpublished data.
(51) Lewis, R. J.; Huang, J. H.; Pecora, R. *Macromolecues*, **1985**, *18*, 944.
(52) Dickerson, R. E. *Sci. Am.* **1983**, *249* (6), 94.
(53) Hagerman, P. J. *Biopolymers* **1983**, *22*, 811.

Atomistic Modeling of Mechanical Properties of Polymeric Glasses

Doros N. Theodorou and Ulrich W. Suter*

Department of Chemical Engineering, Massachusetts Institute of Technology, Cambridge, Massachusetts 02139. *Received June 5, 1985*

ABSTRACT: Methods are developed for the prediction of the elastic constants of an amorphous glassy polymer by small-strain deformation of microscopically detailed model structures. A thermodynamic analysis shows that entropic contributions to the elastic response to deformation can be neglected in polymeric glasses. A statistical mechanical analysis further indicates that vibrational contributions of the hard degrees of freedom are not significant, so that estimates of the elastic constants can be obtained from changes in the total potential energy of static microscopic structures subjected to simple deformations. Mathematical procedures are developed for the atomistic modeling of deformation and applied to glassy atactic polypropylene. Predicted elastic constants are always within 15% of the experimental values, without the use of adjustable parameters. An estimate of the thermal expansion coefficient is also obtained. Inter- and intramolecular contributions to the mechanical properties are examined, and it is found that coexistence in the bulk reduces the effects of individual chain idiosyncrasy.

Introduction

A method for the detailed, atomistic modeling of well-relaxed amorphous glassy polymers has recently been introduced.[1] The polymeric glass was pictured as an ensemble of static microscopic structures in detailed mechanical equilibrium (but not in thermodynamic equilibrium), each microscopic structure being represented by a model cube with periodic boundaries, filled with segments from a single "parent chain". Our modeling approach was applied to glassy atactic polypropylene with very satisfactory results. Model estimates of the cohesive energy and of Hildebrand's solubility parameter agreed very well

* Address correspondence to MIT Chemical Engineering Department, Room 66-456, Cambridge, MA 02139.

0024-9297/86/2219-0139$01.50/0